A High Sensitivity and Low Noise Thermal Gas Flow Sensor Based on Silicon-Doped Thermocouples

Shaogang Hu, Jianping Liu, Haoyuan Zhang, Jinhuan Yin, Yuhang Pu, Liangcheng Tu, and Shanqing Yang

***Abstract*—The detection of gravitational waves in space requires microthrusters that can respond quickly to compensate for nonconservative forces on the satellite with low thrust noise. Flow measurement plays a crucial role in cold gas microthrusters (CGMTs), directly determining the control accuracy of thrust adjustment and the upper limit of thrust noise. It is a challenge to achieve high-resolution and low flow measurement noise for flow measurement to obtain sub-micro-Newtonian thrust resolution and thrust noise. A high-sensitive temperature differential flow sensor has been developed using pairs of doped silicon thermocouples as the key temperature sensing elements. Aiming at reducing the noise at low-frequency band of mHz–Hz, which is the concern of space gravitational waves, the thermal noise of the internal resistance of the thermocouple, the fluctuation noise of the heating power, and the low-frequency noise of the amplifier circuit are carefully handled to achieve a flow measurement noise better than 0.1 μg/s/Hz$^{1/2}$ @ 1 mHz–10 Hz. Through the design of the flow channel, the flow conduction of the system exceeds 10 μg/s/Pa, with a response time of about 10.2 ms, ensuring the rapid response capability. It holds promise for integration into CGMT systems for space-based gravitational wave detection.**

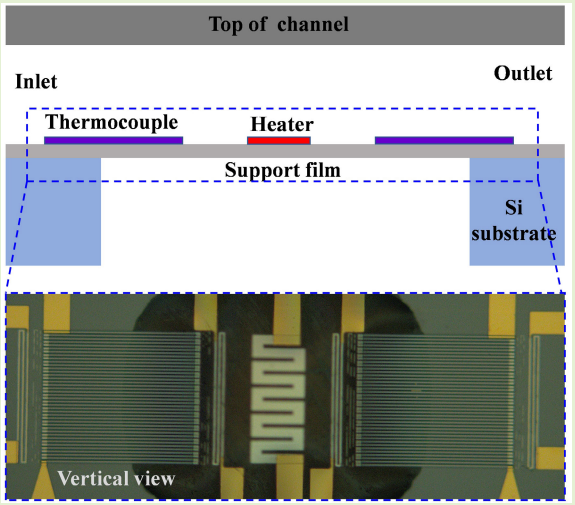

***Index Terms*— Cold gas microthruster, flow measurement, gravitational wave detection, thermocouple.**

I. Introduction

THE detection of gravitational waves plays a pivotal role in the development of novel astronomical observation techniques and the advancement of astrophysics and cosmology [1], [2], [3], [4]. In order to measure low-frequency gravitational wave signals in the mHz range, it is necessary to construct gravitational wave detection platforms in space with million kilometers of arm length [5]. Microthrusters serve as essential actuators for building ultrastable space platforms to counteract the effects of nonconservative forces from internal and external sources [6], [7]. The thrust noise of the microthruster can directly affect the residual acceleration of the test mass through the electrostatic coupling effect between the satellite and the test mass [8]. As a result, several stringent demands on microthrusters are required in space gravitational wave detection as follows: a thrust range of 0–100 μN, a resolution of 0.1 μN, a thrust noise less than 0.1 μN/Hz$^{1/2}$ @ 1 mHz–1 Hz, and a response time of 50 ms [5], [6].

A highly promising microthruster solution, cold gas microthruster (CGMT), has demonstrated excellent performance on laser interferometer space antenna pathfinder (LPF) [9]. According to studies by Matticari et al. [10], Zhang et al. [11], van der List et al. [12], the thrust of CGMT is proportional to the mass flow rate of the exhaust gas. Current CGMT usually uses a closed-loop control based on flow sensing and control valves to achieve a precise control of the gas flow.

Received 19 July 2024; revised 13 September 2024 and 13 October 2024; accepted 5 November 2024. Date of publication 15 November 2024; date of current version 2 January 2025. This work was supported in part by the National Key Research and Development Program of China under Grant 2020YFC2201001 and in part by the National Natural Science Foundation of China under Grant 12105373 and Grant 12105374. The associate editor coordinating the review of this article and approving it for publication was Prof. Sheng-Shian Li. *(Corresponding author: Jianping Liu.)*

The authors are with the MOE Key Laboratory of TianQin Mission, TianQin Research Center for Gravitational Physics, School of Physics and Astronomy, Frontiers Science Center for TianQin, Gravitational Wave Research Center of CNSA, Sun Yat-sen University (Zhuhai Campus), Zhuhai 519082, China (e-mail: hushg3@mail2.sysu.edu.cn; liujp39@mail.sysu.edu.cn; zhanghy275@mail2.sysu.edu.cn; yinjh7@mail2.sysu.edu.cn; puyh5@mail2.sysu.edu.cn; tuliangch@mail.sysu.edu.cn; yshq@mail.sysu.edu.cn).

Digital Object Identifier 10.1109/JSEN.2024.3494801

Therefore, accurate measurement of the mass flow rate of the propellant is critical to achieving high-precision thrust. Since the exhaust velocity is about 500–600 m/s, the requirements for flow rate measurement are as follows: a resolution of 0.2 μg/s, flow rate measurement noise of <0.2 μg/s/Hz$^{1/2}$ @ 1 mHz–1 Hz, and a response time of 20 ms.

Kang et al. investigated the mechanism of thermocouple coefficient reduction and sensor lifespan at high temperatures [13]. A bendable large range heat flow sensor was reported by Li et al. [14] and [15]. The 2-D flow sensor studied by Hartgenbusch et al. [16] achieved an angular resolution of 0.5 °. In order to achieve the high-resolution requirement, the first challenge to be addressed in constructing a flow sensor is to maximize the detection sensitivity of the sensing structure. In CGMT, thermal mass flow sensors (MFSs) are widely applied due to its high-sensitivity and low flow noise. There are two main ways to increase sensitivity: the first is to use materials with a higher temperature coefficient. In the early stages, doped polysilicon and metals were used as thermocouple materials, due to the higher thermoelectric coefficient of semiconductors. Then, the combination of p$^+$Si/Al [17] was found to have higher thermoelectric coefficient as compared with p$^+$poly/metal [18]. Due to advances in processing, thermocouples of two semiconductor materials are widely used, such as p$^+$poly/n$^+$poly [19] and p$^+$Si/n$^+$Si [20], and the sensitivity of the sensors is further enhanced. In addition, increasing the number of thermocouples can also improve the equivalent temperature coefficient of temperature difference measurement, while the internal resistance thermal noise also increases, which limits the maximum number of thermocouples. The parameter Z was used to comprehensively evaluate a pair of thermoelectric materials

$$Z = \frac{\alpha^2}{k\rho_e}$$

where α is Seebeck coefficient, k is thermal conductivity, and ρ_e is electrical resistivity. p$^+$Si/n$^+$Si with higher Z is chosen as the thermocouple material, and its pairs were set to 20 to increase the equivalent temperature coefficient.

The second way to increase sensitivity is to reduce the heat transfer from the temperature measuring and heating elements to the surrounding area and to enhance their heat exchange with the fluid to be measured. Compared with silicon carbide (SC) and silicon nitrite (SN), SiO_2 has a lower thermal conductivity and is more suitable for thermal insulation. Behrmann et al. [21] achieved high-strength thin-film support and minimal thermal insulation loss using atomic layer deposition. Kasai et al. [22] enhanced the insulation of the film by adding holes next to the heater.

Another challenge for flow sensor to meet the demands of gravitational wave detection in space is to achieve ultralow flow measurement noise in the mHz frequency band. Factors affecting the flow measurement noise include the thermal noise of the thermocouple internal resistance, the heating power fluctuation noise, the 1/f noise of the amplifier, and environmental disturbance noise. We analyzed and distributed noise throughout the measurement process and implemented targeted noise suppression measures accordingly. Finally, we achieved that the noise in the wideband of mHz–Hz all met the requirements.

The issue of response time of the CGMT due to the flow conduction of the flow sensor should also be noted. Since it takes time for gas to change state in fixed volume, there is a delay between the flow rate of the gas ejected from the nozzle and the flow rate measured by the sensor, and the time of this delay is inversely proportional to the flow conduction and directly proportional to the volume of the cavity between them [23]. The existence of this delay time makes it difficult to regulate the flow rate, or thrust, quickly and accurately. Since the volume in our CGMT is 2 mL and it is difficult to reduce it significantly, a thrust response time of 50 ms requires the flow conduction of flow sensor, which should be greater than 10 μg/s/Pa.

This article reports a high-resolution and low-noise thermal flow sensor aiming at requirement for space born gravitational wave detection. High system sensitivity combined with peripheral circuit noise suppression results in excellent flow measurement noise characterization in the frequency band of interest. This article is organized as follows. Section II of this article focuses on theoretical analysis and modeling, while Section III discusses the manufacturing of the sensor chip and device construction. The performance test results and analysis are discussed in Section IV. Also, Section V is a summary of the work.

II. Modeling Analysis and Parametric Design

The mass flow sensor (MFS) measures the mass flow rate of fluid by detecting the temperature difference at two specific locations as the fluid passes through the sensor. Its principle is illustrated in Fig. 1. The heating resistor is located at the bottom of the flow channel. Also, two temperature sensing elements are placed symmetrically located at the ends of the heater. As the flow passes over the heater, the gas will carry heat downstream by thermal conduction and convection, resulting in a higher temperature at the downstream temperature sensing point than upstream. The temperature sensing elements and the circuitry convert the temperature difference into voltage signal. In establishing the relationship between the output voltage and the measured flow rate, the model is simplified to a 1-D approximation, and the heat conservation equation can be established as follows:

$$k_f \frac{d^2T(x)}{dx^2} yz\Delta x - \rho cv \frac{dT(x)}{dx} yz\Delta x + k_s \frac{d^2T(x)}{dx^2} ty\Delta x + k_{f1} \frac{d^2T(x)}{dx^2} yh\Delta x = \frac{k_f}{h_c} T(x) y\Delta x + \frac{k_{f1}}{h} T(x) y\Delta x \quad (1)$$

the second term on the left-hand side of the equation represents the heat flux coming in due to convective heat transfer between the fluid and the channel surface. The first, third, and fourth terms represent the heat flux coming in by heat conduction from the flow channel, film, and cavity, respectively. The two items on the right are heat conducted from the side. Equation (1) can be simplified to

$$A \frac{d^2T(x)}{dx^2} + B \frac{dT(x)}{dx} + CT(x) = 0 \quad (2)$$

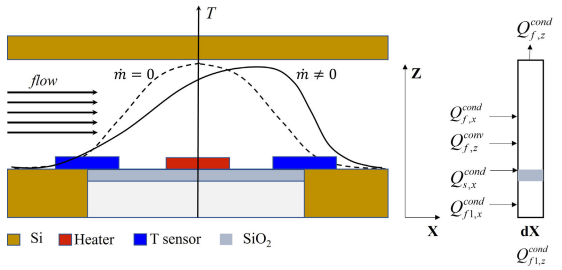

Fig. 1. Differential temperature flow sensing principle diagram. The dashed line shows the distribution curve of temperature in the x-axis direction at zero flow rate, which is symmetrically distributed; the solid line shows that the downstream temperature is higher than the upstream temperature when the flow rate is not zero. The meanings of each parameter are as follows: $Q_{f,z}^{cond}$ heat flowing out of the fluid along the z-direction; $Q_{f,x}^{cond}$ and $Q_{f,x}^{conv}$ net heat flowing into the fluid along the x-direction and net heat flowing through thermal convection, respectively; $Q_{s,x}^{cond}$ net heat conducted into the film along the x-direction; $Q_{f1,x}^{cond}$ net heat conducted into the cavity along the x-direction; and $Q_{f1,z}^{cond}$ net heat flowing out of the cavity through heat conduction in the z-direction.

in which $A = k_s t_s + 1/2\ k_f h_c + 1/2\ k_{f1} h$, $B = -\rho c v z = -\dot{m}c/y$, and $C = -(k_f/h_c + k_{f1}/h)$. k_s and t_s are thermal conductivity and thickness of the film, k_f and h_c are thermal conductivity of the fluid to be measured and height of the flow channel, k_{f1} and h are thermal conductivity of the gas in the cavity and the height of the cavity, and c is heat capacity of the gas.

The boundary conditions are as follows: $T(L) = T(-L) = T_a$, $T(W) = T(-W) = T_h$, T_a is the ambient temperature, T_h is the temperature at the heater, L is the flow path length, and W is half the width of the heater.

Finally, the relationship between the output voltage and the flow rate can be obtained [24]

$$V_{\text{out}} = \alpha \Delta T \left[\frac{e^{xr_2} - e^{r_2 L + r_1 (x-L)}}{e^{r_2 W} - e^{r_2 L + r_1 (W-L)}} - \frac{e^{xr_2} - e^{-r_2 L + r_1 (x+L)}}{e^{-r_2 W} - e^{-r_2 L - r_1 (W-L)}} \right] \tag{3}$$

where $\Delta T = T_h - T_a$, $r_{1,2} = ((-B \mp \sqrt{B^2 - 4AC})/2A)$, and α is the coefficient for temperature conversion to voltage of the temperature sensing element.

Equation (3) can be written as a generalization of the output signal with respect to the flow rate $\dot{m}$ and the temperature difference between the heater and the ambient temperature ΔT

$$V_{\text{out}} = f(\Delta T, \dot{m}). \tag{4}$$

Equation (4) assumes that all other quantities in (3) are fixed. In fact, the geometrical dimensional parameters are fixed, and it is indeed possible that thermodynamic properties, such as thermal conductivity of gases, may change with temperature and pressure, as mentioned in [25]. However, in certain applications, such as the micro-Newtonian CGMT we are targeting, the pressure and temperature of the gas source are stable. Although the pressure in the tanks decreases as the mission progresses, a pressure regulator at the front of the microthruster ensures that the pressure of the gas source is stable, with variations in pressure typically of 0.1% or less. Similarly, the temperature is kept within certain range, and the effect of these two factors on the thermodynamic properties of the gas is negligible in a CGMT.

Equation (4) shows that to achieve a low-noise, ΔT must be stable, and also, the read noise should be focused on as the signal is very weak. In the inherent structure, the thermal resistance from the heater to the environment is fixed, so their temperature difference is proportional to the heating power of the heater P

$$\Delta T \propto P. \tag{5}$$

This condition assumes that the temperature of the gas does not vary over a wide range, and the reasons for temperature stability have been stated in the previous paragraph. The main noise sources are considered to be heating power noise n_P, thermal noise from thermocouples $n_{R_{\text{th}}}$, and noise from amplifier chips n_{op}

$$n_q^2 = n_P^2 + n_{R_{\text{th}}}^2 + n_{\text{op}}^2. \tag{6}$$

The allocation of these three noises with equal weights is a rough estimate at the design stage, in order to initially determine the design parameters. Then, the power noise requirement can be obtained

$$\frac{n_q}{\sqrt{3}\dot{m}_{\max}} = \frac{n_P}{P}. \tag{7}$$

When the heating power is 3.9 mW, the power noise is required to be less than 3.7×10^{-7} W, in which $n_q = 0.05\ \mu\text{g/s/Hz}^{1/2}$ @ 1 mHz–10 Hz and $\dot{m}_{\max} = 300\ \mu\text{g/s}$. Continuing to increase the power will improve the sensitivity, but it also increases the power fluctuation noise, which does not improve the signal-to-noise ratio but increases the power consumption of the system.

To obtain the other two noise requirements, the sensitivity of the system, $S = \partial V_{\text{out}}/\partial \dot{m}$, is first estimated. Obviously, the greater the sensitivity S, the greater the voltage signal at the same flow rate, and the lower the requirement for reading noise. Although thermocouple internal resistance thermal noise is not read noise, they act in the same way, affecting the input of the amplifier.

From (3), it can be observed that the parameters affecting the sensitivity and are easy to control include the dimensions of the channel, the thickness of the thermal insulation layer, and the position of the temperature sensing points. Specific effects of these parameters are provided by thermal simulation using COMSOL for solid and fluid heat transfer. From Fig. 2, it can be seen that as the channel height increases, the temperature difference generated by the flow decreases. This is because, for the same flow rate, increasing the channel height will increase the channel area and reduce the fluid velocity. The temperature difference created by the flow becomes greater as the channel width increases. Although this also leads to a larger channel area and slower flow velocity, the larger thermal conduction area between the fluid and the hotter substrate becomes the dominant factor. Fig. 2(c) shows the smaller the film thickness, the better the insulation, the greater the initial temperature difference between the heater and the environment, and thus, the greater the temperature difference signal generated by the flow. Fig. 2(d) shows that the optimal temperature measurement distance slightly decreases with

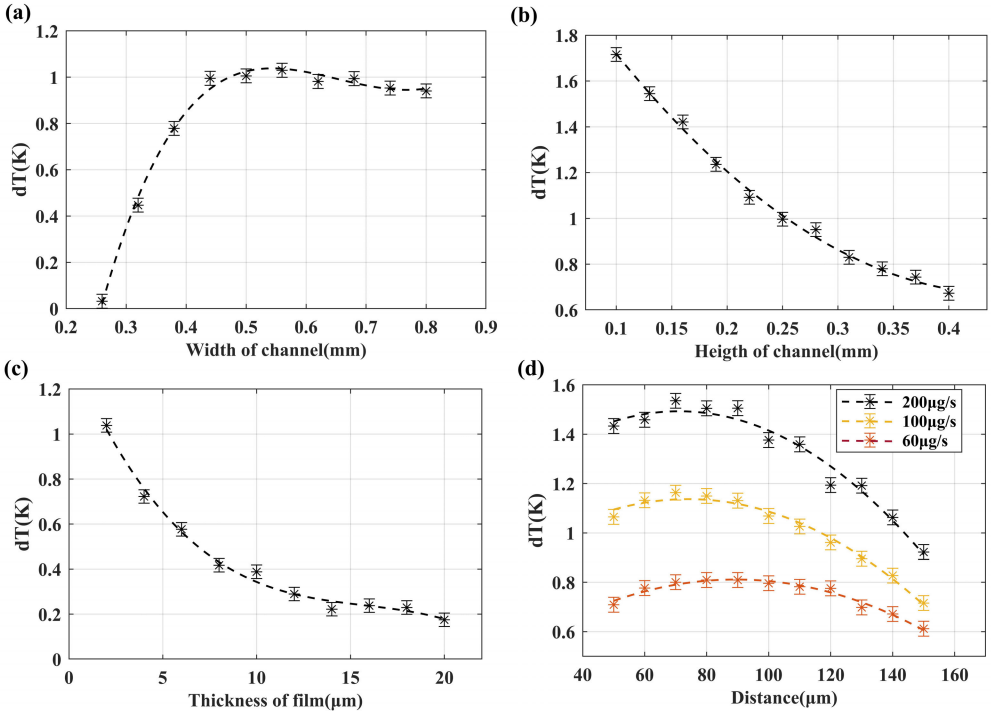

Fig. 2. (a) Influence of channel width on flow signal. (b) Influence of channel height on flow signal. (c) Influence of thermal insulation layer thickness on flow signal. (d) Influence of distance between the temperature measurement point and the heater on flow signal. The optimum distance slightly decreases as the flow rate increases.

TABLE I
DESIGN OF KEY PARAMETERS

Item	Value
Channel height	400 μm
Channel width	600 μm
Film thickness	2 μm
Distance of temperature sensor-heater	80 μm
Heater power	3.9 mW

increasing flow rate. Taking into account the optimal distance for different flow rates, the distance of 80 μm has a high-sensitivity at different flow rates.

It is mentioned in the introduction that due to the response time requirements of the CGMT, the flow conduction of the sensor needs to be greater than 10 μg/s/Pa. In laminar flow conditions, the expression for the flow conduction of a section of the channel is [26]

$$S_c = \frac{q}{\Delta P} = \frac{\pi \rho D_e^4}{128\ \mu L} \tag{8}$$

where μ is the dynamic viscosity of the gas; $D_e = 2ab/(a+b)$ is the equivalent diameter; a and b are the height and width of the rectangular flow path, respectively; ρ is the gas density; and L is the length of the channel. It can be seen that the larger the cross-sectional size of the channel, the greater the flow conduction.

Taking into account the factors, such as the sensitivity of the flow sensing system, flow conduction, and the flow measurement range, the following design parameters are finally proposed as Table I.

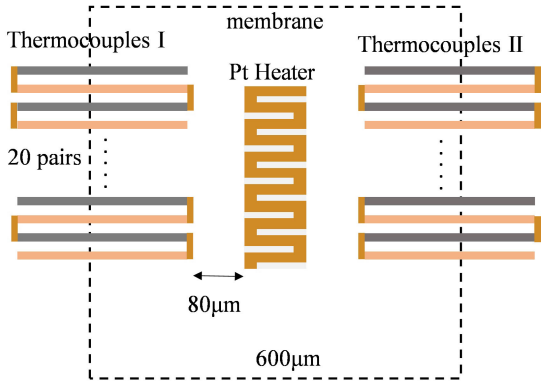

Fig. 3. Dimensional design of platinum heating, two sets of thermocouples, and thermal insulation cavity. The dotted line indicates the extent of the membrane, beneath which a cavity exists.

Serially connecting multiple thermocouples increases the effective temperature coefficient, resulting in a larger voltage signal for the same temperature difference. The cold reference end is placed on the substrate, and subtraction of the output voltages of the two thermocouples also differentials out disturbances caused by changes in ambient temperature. MEMS technology can implement sensing structures in extremely small sizes to maintain sufficient temperature differences for higher system sensitivity. It is important to note that serially connecting multiple thermocouples can result in higher internal resistance, leading to increased thermal noise. The specific design is shown in Fig. 3, where n-type heavily doped silicon and p-type heavily doped silicon are arranged side by side. The heating resistor consists of P_t, which is set into a snake

TABLE II
REQUIREMENT INDICATORS OF VARIOUS NOISES AND THEIR CONTRIBUTIONS TO FLOW NOISE

Noise Source	Value	Equivalent Voltage Noise (10^{-7}V/Hz$^{1/2}$)	Equivalent Flow Rate Noise (μg/s/Hz$^{1/2}$)
Heater power	3.7×10^{-7} W/Hz$^{1/2}$	3.6	0.03
Thermocouple Resistance	3.9 MΩ	3.6	0.03
Amplification Circuit	G=1400	3.6	0.03
All	-	6.24	0.05

shape to increase the heating area, and its resistance value is 80 Ω. The overall length of the heater is 1.45 mm, the width is 20 μm, and the thickness is 0.1 μm. The heater covers an area of 100 × 290 μm.

By means of geometrical parameter design, thermocouple material selection, and multiple pairs of thermocouples connected in series, a design sensitivity of 17.5 mV/μg/s has been achieved. With equal weighted noise assignments, the thermocouple internal resistance thermal noise and readout circuit noise requirements are 3.6×10^{-7} and 3.6×10^{-7} V/Hz$^{1/2}$, respectively, based on a total flow noise requirement of 0.05 μg/s/Hz$^{1/2}$ and design sensitivity. Due to the nonlinear nature of sensitivity, the noise requirement is based on the smallest sensitivity, and it becomes more lenient at higher sensitivities. The noise budget is summarized in Table II. The target noise designed here is 0.05 μg/s/Hz$^{1/2}$, which is better than the actual requirement of 0.2 μg/s/Hz$^{1/2}$ to provide redundancy.

III. CONSTRUCTION OF THE FLOW SENSOR DEVICE

A. Manufacturing of Sensing Chips

The flow sensor chip primarily includes a Si substrate, a thermal insulation cavity, n/p-doped silicon, platinum heating resistor, and platinum connecting lines. Three-layer SOI silicon wafers containing Si, silicon dioxide (SiO_2), and doped silicon are selected as the raw materials. They, respectively, serve as the substrate, thermal insulation layer, and a type of thermoelectric material. The specific processing steps are as follows, as shown in Fig. 4.

1) Commercial SOI silicon wafers are used as the raw material, with a silicon substrate thickness of 500 μm, a SiO_2 layer of 2 μm in the middle, and a 2-μm-thick layer of n-type doped silicon on top.
2) A layer of SiO_2 mask is grown on the SOI silicon wafer as a protective layer, and then, areas requiring p-type doping are etched.
3) P-type silicon doping is performed in the areas where the top SiO_2 mask is unprotected, and then, the top SiO_2 mask layer is removed.
4) Excess n-type doped silicon layer is etched away to isolate the two types of doped silicon.
5) Ti and Pt are alternately plated on the top of the two types of doped silicon. Ti serves to enhance adhesion between the doped silicon and Pt. This process forms multiple serially connected n-Si/p-Si thermocouples. Meanwhile, Pt heating resistors are also plated between the two sets of thermocouples. Gold wires and gold pads are also plated.
6) A thermal insulation cavity is etched on the back of the Si substrate to form the final flow sensing structure.

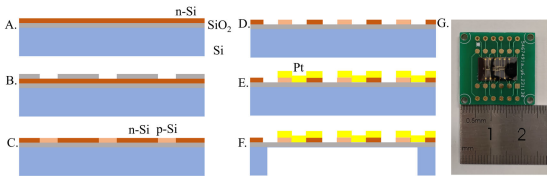

Fig. 4. Manufacturing process of the flow sensor chip. See steps (a)–(f) below for specific steps. (g) Physical image of the flow sensing chip.

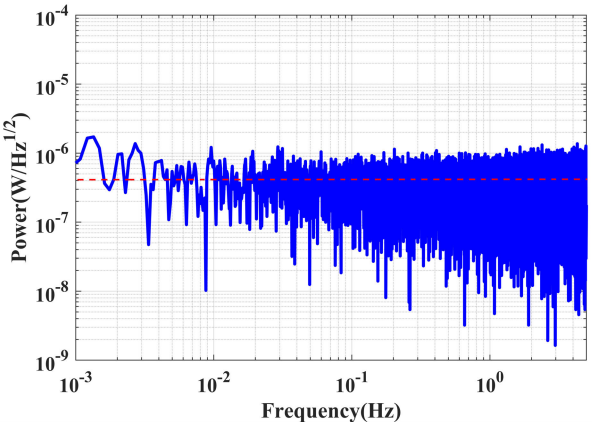

Fig. 5. Heating power noise of the heater @ 3.9 mW with power stabilization circuit.

B. Implementation of Reading and Heating Circuits

In order for the power noise to meet the requirement of $<3.7 \times 10^{-7}$ W/Hz$^{1/2}$ @ 1 mHz–10 Hz, a bridge self-stabilizing circuit is used to compensate for power changes caused by changes in heater resistance, which was also used in [27]. Scale the voltage difference between the two nodes of the bridge, and add it to the power input of the bridge. It is worth noting that the input supply to the bridge also needs to be very stable, and a regulated reference supply (REF330 by TI) is used in the circuit. The level of power control was met, as shown in Fig. 5.

The resistance of a single thermocouple is 600 kΩ, and the thermal noise of two thermocouples is $\sqrt{(4k_bT * 2R)}$, which contributes 0.01 μg/s/Hz$^{1/2}$ to the flow measurement noise. The low-frequency noise of an amplifier typically rises as 1/f, which is unacceptable in readout circuit. To address this issue, TI's OPA187 has excellent noise performance at mHz and does not rise too much compared with the higher frequency bands. The test results show that the voltage noise of the differential amplifier circuit, consisting primarily of OPA187, meets the requirements, as shown in Fig. 6.

C. Sensor System Assembly

As shown in Fig. 7, the flow sensor chip is bonded to a PCB board to connect with the circuit. A flow channel made of

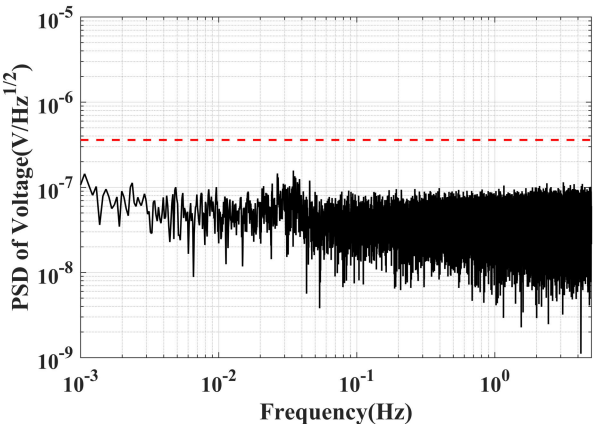

Fig. 6. Readout noise in differential amplifier circuits (pre-op-amp).

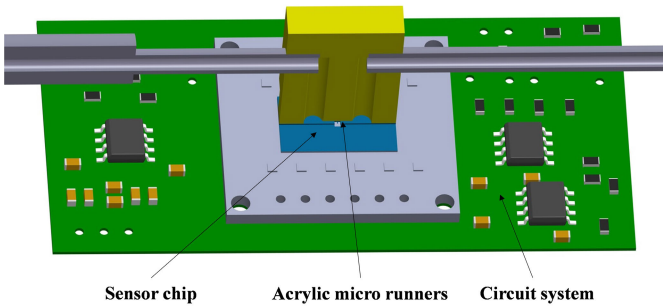

Fig. 7. Schematic illustrating the connection among the flow sensing chip, the flow channel, the circuit board, and the pipeline in the flow sensing device.

acrylic material is attached directly above the chip to facilitate connection with the gas pipeline. At the joints of each part, seal with quick-drying adhesive.

IV. Test Results and Discussion

Calibration of the voltage-flow coefficient of the MFS was conducted by serially measuring gas flow with a commercial flow sensor (Alicat), as shown in Fig. 8. The flow measurement range is from 0 to 350 μg/s, corresponding to voltages ranging from -0.3 to 1.7 V, as shown in Fig. 9. In CGMT, this range enables the generation of thrust of approximately 0–175 μN. As the flow rate increases, sensitivity gradually decreases, ranging from 17.4 to 12.5 mV/μg/s. The normalized sensitivity of 45.78–63.73 mV/sccm/W with respect to the heating power and gain is about 2.29$\times$ better than that of the previously reported thermopile-based gas flow sensor, as listed in Table III. From Fig. 10, it can be observed that the output voltage signal is directly proportional to the heating power, consistent with (3) and (5).

The flow rate resolution of the MFS was tested in a closed-loop configuration, where the voltage output of the MFS was used as a control reference. A square wave flow signal with a period of 2 min and an amplitude of 0.05 μg/s was modulated. Fig. 11 shows that the mass flow measurement resolution of the system is better than 0.05 μg/s. In order to avoid the additional response time associated with closed-loop control, the response time of the system is measured by switching the

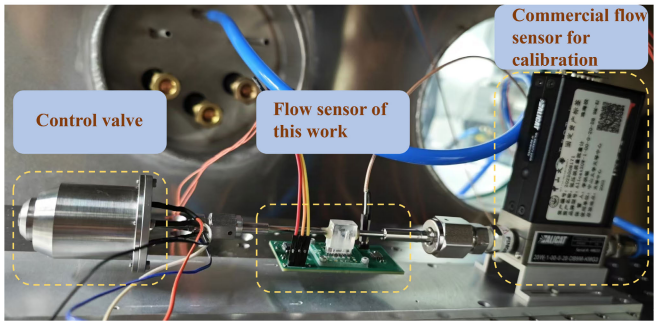

Fig. 8. Overall experimental setup diagram. Control valve is used to regulate flow, and commercial flow sensor is used to calibrate the coefficient of flow sensor output voltage versus flow rate.

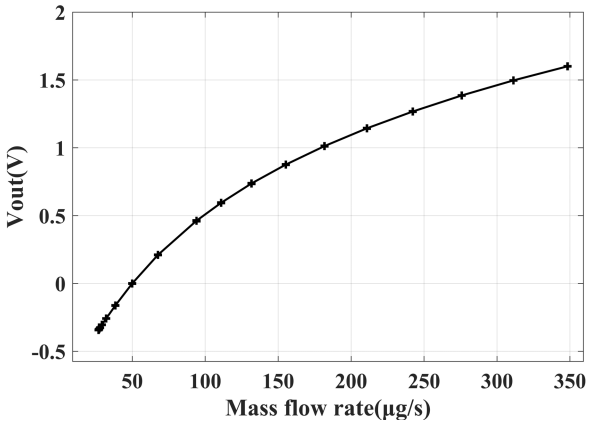

Fig. 9. Relationship between output voltage of MFS and flow rate calibrated against Alicat flow sensor. The sensor's sensitivity ranges from 17.4 to 12.5 mV/μg/s, decreasing as the flow rate increases.

TABLE III
Comparison Between the Reported Thermopile-Based Gas Flow Sensor With Our Work (the Sensitivity in This Table Do Not Take Into Account the Gain of the Amplifier)

Ref.	Area mm^2	Dielectric membrane	Thermocouple materials	Sensitivity mV/(sccm)/W
[17]	17.28	SC-Si-SiO_2	p^+Si/Al	15.80
[28]	0.49	SiN-SiO_2	p^+Si/Au	3.90
[29]	0.35	SiN	p^+Si/Au	0.337
[19]	16	SiO_2	p^+-Poly/n^+-Poly	20.00
[20]	0.39	SiN	p^+Si/n^+Si	16
Our work	84	SiO_2	p^+Si/n^+Si	45.78-63.73

heater. The rise time of the flow measurement signal from switching the heater off to on at a fixed flow rate represents the time required for the system to thermally stabilize or the measured response time of the system. We measured the response time at a flow rate of 10–360 μg/s and found that the response time decreases slightly as the flow rate increases, thus evaluating the response time to be approximately 10.2 ms, as shown in Fig. 12. In the experiment, the measured value of the flow conduction is 12 μg/s/Pa, which satisfies the need for 10 μg/s/Pa.

When measuring the measurement noise of the MFS, the piezoelectric valve at the back end is held constant at a fixed

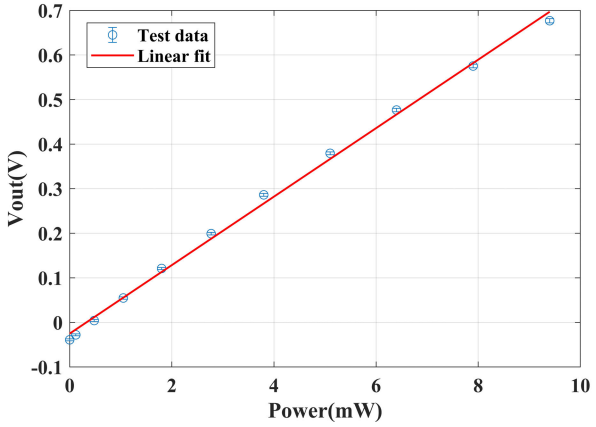

Fig. 10. Relationship between voltage signal and heating power at fixed flow rates. The output voltage is proportional to the heating power.

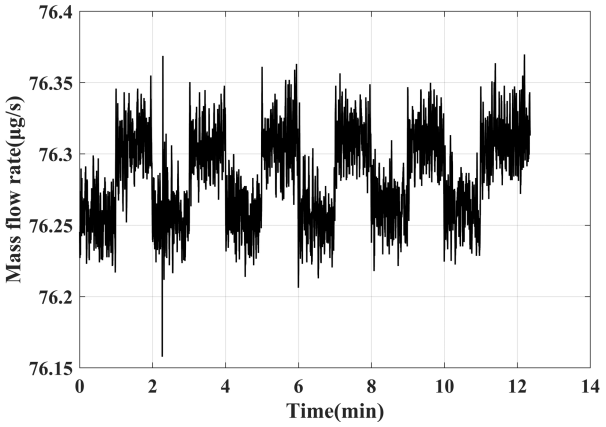

Fig. 11. Measurement results of a flow signal with a period of 2 min and an amplitude of 0.05 μg/s, demonstrating that the system measurement resolution is better than 0.05 μg/s.

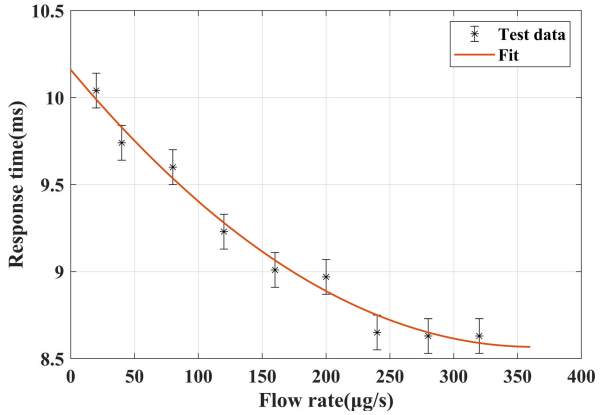

Fig. 12. Response time decreases slightly as the flow rate increases, and response time is about 10.2 ms.

opening, and the gas supply to the air inlet is at a pressure of 1 bar. The flow noise measured in this way includes both the noise of the flow sensor and the noise of the flow caused by changes in the pressure of the gas source and fluctuations in the opening of the valve. With the noise results shown in Fig. 13, it can be concluded that the noise of the flow sensor is

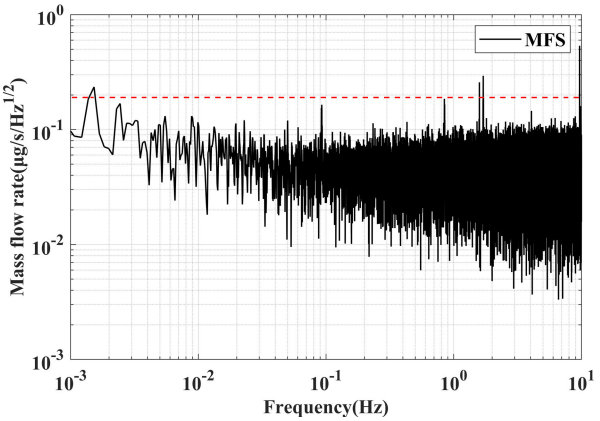

Fig. 13. Flow measurement noise at a fixed flow rate, including both the fluctuation noise of the and the noise of the sensor. The results indicate that the sensor noise is better than 0.1 μg/s/Hz$^{1/2}$ @ 1 mHz–10 Hz.

better than 0.1 μg/s/Hz$^{1/2}$ @ 1 mHz–10 Hz. The corresponding thrust noise level is approximately 0.05 μN/Hz$^{1/2}$ in the same frequency range, which meets the noise requirement of CGMT used in space gravitational wave detection.

V. Conclusion

In response to the requirements of space gravitational wave detection, a high-resolution, low-noise thermal MFS has been designed, manufactured, and tested. MEMS technology was used to manufacture the sensitive components of the flow sensor. Fine physical modeling and noise distribution of the entire flow measurement process were performed. Based on the principle of sensitivity maximization, the design of parameters, such as flow channel dimensions, membrane thickness, and temperature measurement distance, was optimized. To address low-frequency flow measurement noise, 20 pairs n^+Si/p^+Si thermocouple material and SiO_2 insulation were used to improve system sensitivity; low-frequency power noise from the heater was suppressed, and a low-noise amplifier was used.

The experimental results show that the following performances were achieved: flow measurement range: 0–350 μg/s, flow measurement resolution: 0.05 μg/s, flow measurement response time is about 10.2 ms, flow measurement noise better than 0.1 μg/s/Hz$^{1/2}$ @ 1 mHz to 10 Hz, and flow conduction greater than 12 μg/s/Pa. These performance metrics meet the requirements for flow sensing in CGMT used in space gravitational wave detection.

References

[1] B. P. Abbott et al., "GWTC-1: A gravitational-wave transient catalog of compact binary mergers observed by LIGO and Virgo during the first and second observing runs," *Phys. Rev. X*, vol. 9, no. 3, 2019, Art. no. 031040.

[2] H.-T. Wang et al., "Science with the TianQin observatory: Preliminary results on massive black hole binaries," *Phys. Rev. D, Part. Fields*, vol. 100, no. 4, Aug. 2019, Art. no. 043003.

[3] M. R. Adams, N. J. Cornish, and T. B. Littenberg, "Astrophysical model selection in gravitational wave astronomy," *Phys. Rev. D, Part. Fields*, vol. 86, no. 12, Dec. 2012, Art. no. 124032.

[4] C. Caprini and D. G. Figueroa, "Cosmological backgrounds of gravitational waves," *Classical Quantum Gravity*, vol. 35, no. 16, Aug. 2018, Art. no. 163001.

[5] J. Luo et al., "TianQin: A space-borne gravitational wave detector," *Classical Quantum Gravity*, vol. 33, no. 3, Feb. 2016, Art. no. 035010.

[6] J. Ziemer et al., "LISA colloid microthruster technology development plan and progress," in *Proc. 36th Int. Electric Propuls. Conf.*, 2019, pp. 1–15.

[7] J. Luo et al., "The first round result from the TianQin-1 satellite," *Classical Quantum Gravity*, vol. 37, no. 18, 2020, Art. no. 185013.

[8] B. L. Schumaker, "Disturbance reduction requirements for LISA," *Classical Quantum Gravity*, vol. 20, no. 10, pp. 239–253, May 2003.

[9] A. Schleicher et al., "In-orbit performance of the LISA pathfinder drag-free and attitude control system," *CEAS Space J.*, vol. 10, no. 4, pp. 471–485, Dec. 2018.

[10] G. Matticari, G. Noci, P. Siciliano, G. Colangelo, and R. Schmidt, "Cold gas micro propulsion prototype for very fine spacecraft attitude/position control," in *Proc. 42nd AIAA/ASME/SAE/ASEE Joint Propuls. Conf. Exhib.*, Jul. 2006, p. 4872.

[11] H.-Y. Zhang et al., "A high resolution and wide range valve for micronewton cold gas thrusters," *Rev. Scientific Instrum.*, vol. 95, no. 2, Feb. 2024, Art. no. 024501.

[12] M. van der List, P. van Put, V. Yüce, and J. Kuiper, "Next generation electrical propulsion feed systems and spin-off micro-propulsion components," in *Proc. 42nd AIAA/ASME/SAE/ASEE Joint Propuls. Conf. Exhib.*, Jul. 2006, p. 4848.

[13] Q. Kang, Y. Lin, and J. Tao, "Performance of a MEMS flow sensor with high-temperature," *IEEE Sensors J.*, early access, May 20, 2024, doi: 10.1109/JSEN.2024.3396078.

[14] M. Li et al., "Fabrication and characterization of high-sensitivity, wide-range, and flexible MEMS thermal flow velocity sensors," *Microsyst. Nanoeng.*, vol. 10, no. 1, p. 102, Jul. 2024.

[15] K. Xu et al., "Laser direct writing of flexible thermal flow sensors," *Nano Lett.*, vol. 23, no. 22, pp. 10317–10325, Nov. 2023.

[16] N. Hartgenbusch, M. Borysov, R. Jedermann, and W. Lang, "Characterization and design evaluation of membrane-based calorimetric MEMS sensors for two-dimensional flow measurement," *IEEE Sensors J.*, vol. 20, no. 9, pp. 4602–4609, May 2020.

[17] D. Randjelović et al., "Multipurpose MEMS thermal sensor based on thermopiles," *Sens. Actuators A, Phys.*, vol. 141, no. 2, pp. 404–413, Feb. 2008.

[18] R. Buchner, C. Sosna, M. Maiwald, W. Benecke, and W. Lang, "A high-temperature thermopile fabrication process for thermal flow sensors," *Sens. Actuators A, Phys.*, vols. 130–131, pp. 262–266, Aug. 2006.

[19] P. Bruschi, M. Dei, and M. Piotto, "A single chip, double channel thermal flow meter," *Microsyst. Technol.*, vol. 15, no. 8, pp. 1179–1186, Aug. 2009.

[20] P. Zhang, T. Huang, J. Wang, and X. Li, "Single (111)-wafer single-side microfabrication of suspended p+Si/n+Si thermopile for tiny-size and high-sensitivity thermal gas flow sensors," *IEEE Sensors J.*, vol. 23, no. 6, pp. 5628–5636, Mar. 2023.

[21] O. Behrmann, T. Lisec, S. Billat, A. Dehe, and B. Gojdka, "Influence of a novel solid thermal isolation material for MEMS on thermopile sensitivity and dynamic response of a MEMS flow sensor," in *Proc. MikroSystemTechnik Kongress*, 2023, pp. 787–790.

[22] T. Kasai, K. Momotani, Y. Nakano, and H. Nakao, "Improvement of thermal-type MEMS flow sensor chip via new process of silicon etching with sacrificial polycrystalline silicon layer," *Electr. Eng. Jpn.*, vol. 214, no. 4, 2021, Art. no. e23352.

[23] T. Lienart, "First in-flight observations of the cold gas propulsion system for CNES' microscope spacecraft," in *Proc. 53rd AIAA/SAE/ASEE Joint Propuls. Conf.*, Jul. 2017, p. 4947.

[24] W. Xu, K. Song, S. Ma, B. Gao, Y. Chiu, and Y.-K. Lee, "Theoretical and experimental investigations of thermoresistive micro calorimetric flow sensors fabricated by CMOS MEMS technology," *J. Microelectromech. Syst.*, vol. 25, no. 5, pp. 954–962, Oct. 2016.

[25] P. Bruschi, M. Dei, and M. Piotto, "A method to compensate the pressure sensitivity of integrated thermal flow sensors," *IEEE Sensors J.*, vol. 10, no. 10, pp. 1589–1597, Oct. 2010.

[26] L. D. Landau and E. M. Lifshitz, *Fluid Mechanics: Landau and Lifshitz: Course of Theoretical Physics*, vol. 6. Amsterdam, The Netherlands: Elsevier, 2013.

[27] W. Xu, S. Ma, X. Wang, Y. Chiu, and Y.-K. Lee, "A CMOS-MEMS thermoresistive micro calorimetric flow sensor with temperature compensation," *J. Microelectromech. Syst.*, vol. 28, no. 5, pp. 841–849, Oct. 2019.

[28] D. Xue, J. Wang, and X. Li, "A front-side microfabricated thermoresistive gas flow sensor for high-performance, low-cost and high-yield volume production," *Micromachines*, vol. 11, no. 2, p. 205, Feb. 2020.

[29] S. Wang, J. Wang, and X. Li, "Sensitivity improvement of P+Si/Au thermopile-based gas flow sensor by optimizing heat-sink and thermal-insulation configuration," in *Proc. IEEE 33rd Int. Conf. Micro Electro Mech. Syst. (MEMS)*, Jan. 2020, pp. 657–660.

Shaogang Hu received the master's degree from the Department of Physics, Huazhong University of Science and Technology, Wuhan, China, in 2021. He is currently pursuing the Ph.D. degree with the School of Physics and Astronomy, Sun Yat-sen University, Zhuhai, China.

His research interests include flow sensor and micropropulsion research.

Jianping Liu received the Ph.D. degree from the Department of Physics, Huazhong University of Science and Technology, Wuhan, China, in 2019.

He is currently an Associate Research Fellow at Sun Yat-sen University, Zhuhai, China. His research interests include precision measurement, gravitational experiments, gravitational wave detection, and micropropulsion research.

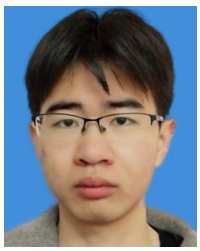

Haoyuan Zhang received the bachelor's degree from the School of Physics, Huazhong University of Science and Technology, Wuhan, China, in 2019. He is currently pursuing the Ph.D. degree with The Tian-Qin Research Center for Gravitational Physics, Sun Yat-sen University, Zhuhai, China.

His research interests include micro-Newton cold gas thrusters, high-precision flow control valve development, and nonlinear flow control.

Jinhuan Yin received the bachelor's degree from the School of Materials and Energy and the School of Integrated Circuits, Guangdong University of Technology, Guangzhou, China, in 2022. He is currently pursuing the master's degree with The Tian-Qin Research Center for Gravitational Physics, The Sun Yat-sen University, Zhuhai, China.

His research interests include fluid dynamics, nonequilibrium thermodynamics, molecular dynamics simulations, and Laval nozzle's design research.

Yuhang Pu received the bachelor's degree from the School of Space Science and Technology, Shandong University, Weihai, China, in 2023. He is currently pursuing the master's degree with The Tian-Qin Research Center for Gravitational Physics, The Sun Yat-sen University, Zhuhai, China.

His recent research focuses on the study of environmental disturbance and packaging design of cold gas micropropulsion.

Liangcheng Tu received the B.S. degree in physical science from Hubei University, Wuhan, China, in 1996, and the Ph.D. degree in physical science from Huazhong University of Science and Technology, Wuhan, in 2006.

He is currently a Full-Time Professor with the School of Physics and Astronomy, Sun Yat-sen University, Zhuhai, China. His current research interests include gravity measurement technologies, space gravitational wave detection, universal time measurement, semiconductor device physics, and related fields.

Shanqing Yang received the Ph.D. degree from Huazhong University of Science and Technology, Wuhan, China, in 2009.

He is currently a Professor with the School of Physics and Astronomy, Sun Yat-sen University, Zhuhai, China. He has long been engaged in the precise testing of Newton's law of gravitation and the application of torsion balance technology. His major achievements include the following: internationally, he was the first to accurately measure the impact of the anelastic effect of tungsten wire on the measurement of the gravitational constant G using the torsion balance period method, providing a quantitative explanation to the long-standing debate on this issue. By utilizing a precision torsion balance, he significantly improved the experimental accuracy of testing Newton's inverse-square law at close distances by several folds, setting stricter constraints for theoretical research on extra dimensions and other related topics. Together with his team, he employed two methods to measure the gravitational constant G with the highest precision achieved internationally to date, which has been recognized and included by the Committee on Data for Science and Technology (CODATA). He has co-authored more than 70 articles, including one in *Nature* and eight in *Physical Review Letters* (PRL).